

# Ferroelectric Aluminum Scandium Nitride Thin Film Bulk Acoustic Resonators with Polarization-Dependent Operating States

Jialin Wang, Yue Zheng, and Azadeh Ansari\*

Given the recent discovery of ferroelectricity in highly doped AIN films and their widespread use in bulk acoustic wave (BAW) filters, the ferroelectric and acoustic performance of AlScN-based devices at two distinct polarization states, i.e., nitrogen (N)-polar and metal-polar states, is investigated. Unreleased metalferroelectric-metal (MFM) capacitors, as well as suspended MFM structures in the form of thin-film bulk acoustic resonators (FBARs), are fabricated based on Mo/AlScN/Mo-sputtered films with  $\approx$ 30% Sc concentration. The hysteresis polarization-electric field (P-E) loops and internal resistance of the MFM capacitors are characterized. The FBAR devices are characterized at the two polarization states, where the polarization inversion is accompanied by the modulation of thin-film stress and resistance. Furthermore, the as-fabricated N-polar FBAR shows a fundamental thickness-mode resonance frequency of 3.17 GHz, with a quality factor (Q<sub>Bode</sub>) of 572 and a high effective electromechanical coupling coefficient  $(k_t^2)$  of 11.4%. The FBAR frequency response changes when the polarization is switched from N-polar to metal-polar. Herein, the first investigations of electric and acoustic properties of N-polar and metalpolar AIScN-based devices are demonstrated, paving the way for the realization of high-k<sub>t</sub><sup>2</sup>-reconfigurable acoustic filters for next-generation communication systems operating at the super-high-frequency (SHF) range.

## 1. Introduction

Due to their unique behavior, ferroelectric materials have accrued increasing research attention in a variety of fields, including nonvolatile memory<sup>[1,2]</sup> and reconfigurable acoustic filters.<sup>[3]</sup> They provide a unique intrinsic polarization switching capability due to the existence of two polarization states with different remnant polarizations. Such materials can also possess two distinct resistance states, which can be switched by applying a bias electric field greater than the coercive field.<sup>[4]</sup> Other unique behaviors such as dielectric constant modulation with applied bias and negative capacitance upon polarization inversion have

J. Wang, Y. Zheng, Prof. A. Ansari School of Electrical and Computer Engineering Georgia Institute of Technology Atlanta, GA, USA E-mail: azadeh.ansari@ece.gatech.edu

The ORCID identification number(s) for the author(s) of this article can be found under https://doi.org/10.1002/pssr.202100034.

DOI: 10.1002/pssr.202100034

been demonstrated on other ferroelectric materials such as PZT and hafnium oxide  $(HfO_2)$ . [5,6]

Several approaches have been taken to develop switchable acoustic devices with various ferroelectric and paraelectric materials, such as PZT<sup>[3,7]</sup> and BST.<sup>[8]</sup> However, most of the acoustic devices based on PZT and BST have several limitations, including limited Q factor, a lack of complementary metal-oxide-semiconductor (CMOS)-compatible fabrication processes, and a DC bias requirement to turn on the device in the case of BST.[9-11] Recently, ferroelectric properties have been discovered in thin-film aluminum scandium nitride (Al<sub>1-x</sub>Sc<sub>x</sub>N) with x > 27%. [12] Due to the infancy of the field, a fundamental study of various mechanisms that are a result of polarization switching in ferroelectric-doped AlN films has not been conducted to date. Despite the popularity of AlN-based acoustic devices, the added ferroelectric properties of the films with high Sc content have not been explored for radio-frequency signal-processing applica-

tions. AlScN-based acoustic devices have the advantages of high Q factor compared to PZT-based ferroelectric resonators, <sup>[3]</sup> high  $k_{\rm t}^2$  because of the increase in the piezoelectric coefficient ( $e_{33}$ ) in highly doped AlN films, <sup>[13]</sup> and high operating temperatures due to the wide bandgap. <sup>[14–16]</sup> The additional tuning and polarization switching properties offered by the ferroelectric AlScN can provide a path forward for the realization of reconfigurable filters in the next-generation wireless communication devices.

In this work, the ferroelectric behavior of an  $\mathrm{Al}_{1-x}\mathrm{Sc}_x\mathrm{N}$  thin film with  $x\approx0.3$  is first characterized, showing a square-like polarization—electric field (P-E) loop. The resistance switching behavior for both the parallel resistance  $(R_\mathrm{p})$  and the equivalent series resistance (ESR) of the thin film is then studied, showing two distinct resistance states [17,18] for N-polar and metal-polar films. Finally, two operating states of the FBAR are studied by measuring the admittance  $(Y_{11})$  frequency response of the as-fabricated  $\mathrm{Al}_{0.7}\mathrm{Sc}_{0.3}\mathrm{N}$ -based FBAR (N-polar) and after a unipolar bias voltage with an amplitude greater than the coercive field is applied and removed (metal-polar). The FBAR demonstrated two operating states depending on the resistance states, which modulated the intensity of the admittance  $(Y_{11})$  response and the suspended thin film static deformation, and hence



modulated the  $k_{\rm t}^2$  of the Y<sub>11</sub> response. The static deformation of the suspended film, induced by the residual stress accumulation during the polarization switching process, is believed to cause the change in  $k_{\rm t}^2$ .<sup>[19]</sup>

#### 2. Fabrication Process

The metal-ferroelectric-metal (MFM) capacitor with the structure of molybdenum (Mo)/Al<sub>0.7</sub>Sc<sub>0.3</sub>N/Mo and thicknesses of 110 nm/880 nm/100 nm, respectively, was sputtered on a silicon-on-insulator (SOI) substrate at VTT Technical Research Centre of Finland. Figure 1a,b shows a cross-sectional scanning electron microscopy (SEM) image and the schematic of the unreleased MFM capacitor. The MFM capacitor was fabricated by etching down the top Mo layer with reactive ion etching (RIE) under SF<sub>6</sub>-based chemistries. The Al<sub>0.7</sub>Sc<sub>0.3</sub>N ferroelectric layer was etched via an inductively coupled plasma (ICP) ion-etching tool with chlorine-based chemistry. The Al<sub>0.7</sub>Sc<sub>0.3</sub>N-based FBAR was fabricated on the same sputtered sample, where the Si device layer was etched with xenon difluoride (XeF<sub>2</sub>). Figure 1c,d shows the cross-sectional schematic of the fabricated FBAR. The detailed fabrication processes are discussed in various studies.[20,21]

## 3. AlScN Thin-Film Characterization

#### 3.1. Fatigue in AlScN Ferroelectric Films

Similar to other ferroelectric materials such as  $HfO_2$  and PZT, AlScN P-E loops demonstrate different states as the bias time increases. <sup>[1,22–24]</sup> The periodic polarization switching used to obtain P-E loops is achieved by applying a triangular waveform with a frequency of 1 kHz and a peak voltage of 300 V (**Figure 2a**). Figure 2b shows measured P-E loops under various switching cycles. Figure 2c shows the remnant polarization versus the number of cycles with the applied switching bias.

The P-E loop of the MFM capacitor behaves in three regimes. The first is referred to as the "wake-up" stage and is observed as an increase of the difference between the two remnant polarizations with increasing bias cycling time. [22] In this stage, the increase in the gap between positive and negative remnant polarization is caused by depinching, resulting from the gradual decrease of the built-in bias field. [23] The second stage of the P-E loop is the "normal operation" stage, where the difference between the two remnant polarizations remains constant with increasing cycles. The final stage of the P-E loop is the "fatigue" stage, where the difference in remnant polarization reduces with higher number of cycles. The fatigue is due to the degradation of

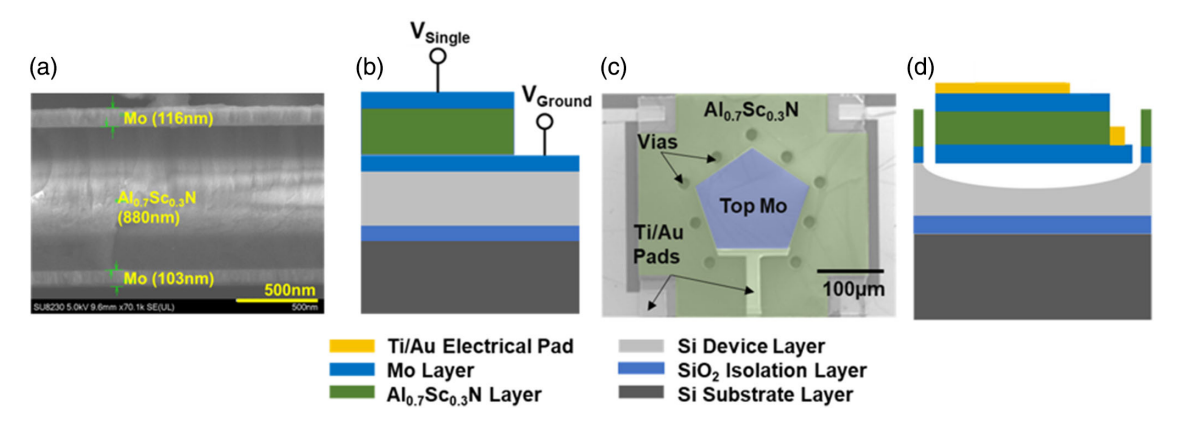


Figure 1. a) Cross-sectional SEM image and b) the schematic of the sputtered MFM capacitor on an SOI substrate. c) SEM image of the fabricated FBAR and d) cross-sectional schematic of FBAR released from the front side with an isotropic etching of the Si device layer.

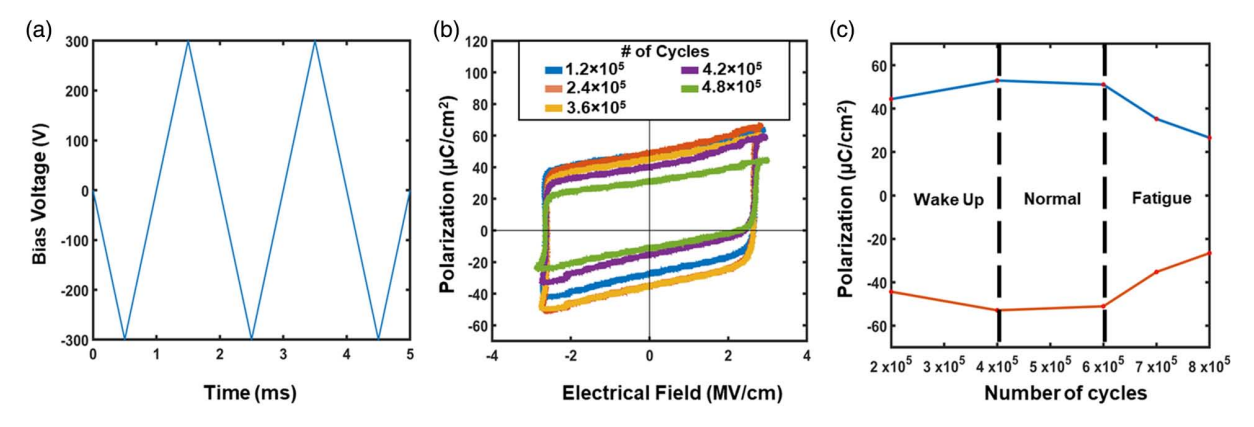


Figure 2. a) Triangular waveform used to obtain P-E loop measurements in the S-T circuit with a frequency of 1 kHz and peak voltage of 300 V. b) The evolution of polarization in ferroelectric AlScN MFM capacitors with increasing the number of switching cycles. c) Remnant polarization versus number of switching cycles, showing wake-up, normal, and fatigue states.



www.advancedsciencenews.com www.pss-rapid.co



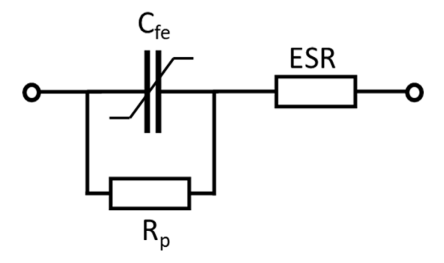


Figure 3. Circuit diagram for modeling the MFM capacitor.

the ferroelectric behavior in the thin film, which leads to a reduction of the remnant polarization during bipolar electric cycling. The ideal operating lifespan for the switchable FBAR could be determined by careful characterization of the "wake up" and "fatigue" stages of the thin films. For the  $Al_{0.3}Sc_{0.7}N$ -based thin film, the fatigue stage occurs after around  $3.8\times10^5$  cycles, which is higher than other ferroelectric thin films such as HfO<sub>2</sub>. This is indicative of a longer lifespan than other ferroelectric-based devices. [1]

#### 3.2. Resistance Change in N-polar and Metal-Polar AlScN

**Figure 3** shows the simple circuit diagram for modeling the MFM capacitor, which includes a parallel capacitor ( $C_p$ ), a parallel resistor ( $R_p$ ), and an ESR. **Table 1** shows the behavior of  $R_p$  at two stages: as-fabricated (N-polar) and after polarization inversion (by application and removal of  $-300\,\mathrm{V}$  DC bias, metalpolar).  $R_p$  of the MFM capacitor enters a low resistance state (LRS) or a high resistance state (HRS) depending on the biasing voltage polarity. The cause for the LRS and HRS is attributed to the switching of the orientation of the dipoles within the  $\mathrm{Al}_{0.7}\mathrm{Sc}_{0.3}\mathrm{N}$  ferroelectric thin film. The different polarizations of the  $\mathrm{Al}_{0.7}\mathrm{Sc}_{0.3}\mathrm{N}$  thin film will either oppose (N-polar) or assist (metal-polar) the current flow, which will determine the resistance state of the film.

The change in ESR is measured at room temperature, with the result shown in Table 1. Unlike the  $R_{\rm p}$ , ESR increases after polarization switching from N-polar to metal-polar and decreases after the polarization is switched back to N-polar. This behavior is attributed to both the imperfect-screening effect and the space—charge effect of the ferroelectric thin film during polarization switching. The two effects of the thin film lead to an increase in the energy barrier between the metal—ferroelectric interface after applying a negative bias, [18] causing an increase in the ESR after polarization switching.

**Table 1.** Parameter values extracted from C-V measurement of the MFM at 1 MHz

Circuit Components	As fabricated (N-polar)	After first polarization switching (metal-polar)		
$R_{\rm p} [{\rm M}\Omega]$	704.469	218.2917		
$ESR\ [k\Omega]$	10.18917	28.93927		
C <sub>fe</sub> [pF]	12.3	12.62		

## 4. FBAR Frequency Characterization

The Al<sub>0.7</sub>Sc<sub>0.3</sub>N-based FBAR was fabricated on the same SOI substrate as the MFM capacitor. The FBAR device fabrication only requires an additional release step to form suspended Mo/AlScN/Mo structures. The Y<sub>11</sub> admittance was measured with a Keysight N54244B PNA network analyzer. The polarization and internal resistance switching of the FBAR were achieved by applying a unipolar triangular wave with the negative peak voltage greater than the coercive field (-300 V) at 100 Hz. [26] The polarization of the FBAR could also be switched back with the same triangular waveform but a positive peak voltage of 300 V. [20] Figure 4a,b shows the intensity of the measured, modified Butterworth-Van Dyke (mBVD)-fitted, and de-embedded admittance (Y11) responses of the FBAR for three cases of: 1) as-fabricated (pristine), 2) after first polarization inversion to metal-polar film (after applying a unipolar triangle bias at 1 kHz with a peak voltage of negative 300 V for 6 s), which leads to a decrease in  $R_p$  and an increase in ESR, and 3) after the polarization is switched back to N-polar (after applying a unipolar triangle bias at 1 kHz with a peak voltage of positive 300 V for 6 s), which leads to an increase in  $R_p$  and a decrease in ESR. The effective operating state change of the FBAR manisfests as the drop of the  $k_t^2$ ,  $Q_{\text{Bode}}$ , and the intensity of the  $Y_{11}$  plot. The  $k_t^2$  and  $Q_{\text{Bode}}$ of the FBAR are calculated by Equation (1) and (2). [19,24]

$$k_{\rm t}^2 = \frac{\pi^2}{4} \times \frac{f_{\rm s}(f_{\rm p} - f_{\rm s})}{f_{\rm p}^2} \tag{1}$$

$$Q_{\text{bode}} = \omega |S_{11}| \times \frac{\text{group}_{\text{delay}(S_{11})}}{1 - |S_{11}|^2}$$
 (2)

 $f_{\rm s}$  is the series resonant frequency,  $f_{\rm p}$  is the parallel resonant frequency, and  $S_{11}$  is the return loss of the scattering parameter measurement result of the FBAR.  $k_{\rm t}^2$  and the  $Q_{\rm Bode}$  of the FBAR dropped from 11.4% to 3.76% and 572 to 107, respectively, upon polarization inversion, which demonstrated that the FBAR changes to another state after polarization inversion. The operating frequency of the FBAR could also be effectively tuned back once the polarization is switched back to the N-polar state with a positive bias.

The mBVD model, shown in Figure 4c, is used to analyze the Y<sub>11</sub> response of the FBAR before and after the polarization and the resistance switching with the extracted parameter shown in Table 2. An extra parallel capacitor is used in the mBVD circuit to model the extra parasitic parallel capacitance between the signal and ground pads present in our fabricated devices. Two different behaviors, including the decrease in the  $Y_{11}$  intensity and the  $k_t^2$ , were observed when the FBAR changed operating states. The mBVD model is used to analyze both behaviors by fitting Y<sub>11</sub> of the FBARs. The mBVD model for FBAR after polarization inversion was fit by changing Ro, Rs, Lm, and Cm. The decreased intensity of the FBAR could be attributed to the change of resistance state.  $R_0$  of the model decreased, and  $R_s$  increased after polarization inversion, which matches the experiment results from the MFM capacitor discussed in Section 3. The resistances in the mBVD model are much lower compared to the low-frequency measurement, which is a result of the resistance reduction with increasing frequency as shown in Equation (3).[27]



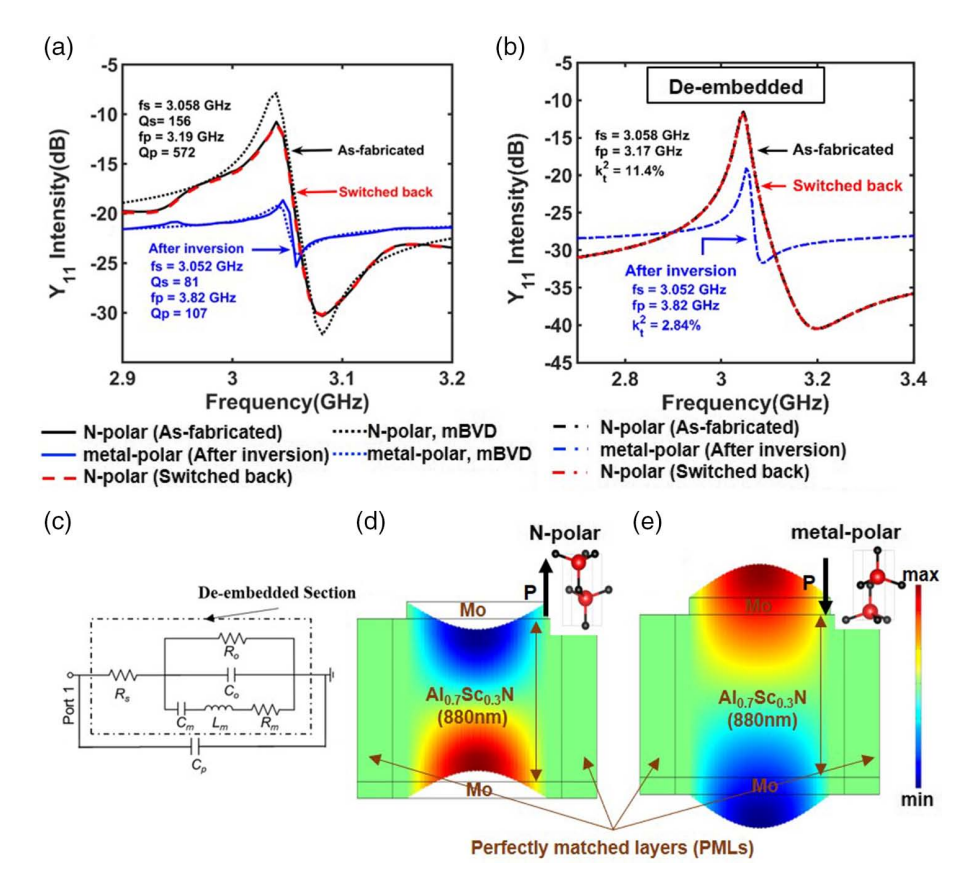


**Figure 4.** a) Magnitude of the measured and mBVD-simulated  $Al_{0.7}Sc_{0.3}N$ -based FBAR admittance ( $Y_{11}$ ) with multiple polarization switching cycles; b) de-embedded admittance response of the FBAR under two polarization states; and c) circuit diagram of the mBVD model used to fit the measured data. d,e) The polarization direction and COMSOL-simulated displacement at the resonant frequency for the N-polar (as-fabricated) state (d) and metal-polar (after polarization inversion) (e). The deformation of the thin film is reversed when the polarization is switched from N-polar to metal-polar.

Table 2. mBVD model parameters for FBARs at two polarization states.

mBVD model	$R_{s} [\Omega]$	$R_{\circ} [\Omega]$	C <sub>o</sub> [fF]	C <sub>m</sub> [fF]	L <sub>m</sub> [nH]	$R_{m}\left[\Omega\right]$	C <sub>p</sub> [fF]
As-fabricated (N-polar)	2.5	110	1100	111	24.7	1.3	3700
After polarization switching (metal-polar)	11.5	30	1100	34	80.2	1.3	3700

$$ESR = \frac{k_{\rm s}}{f} + ESR_{\rm o} \tag{3}$$

where  $k_{\rm s}$  is a constant with a unit of  $\Omega$ Hz, f is the measured frequency, and ESR<sub>o</sub> is the minimum value of the ESR.  $k_{\rm t}^2$  of the FBAR also dropped by about 60% once the FBAR changed to the other operation state. The drop in  $k_{\rm t}^2$  is attributed to the change in the planar residual stress in the thin film after polarization switching. It has been shown that the thin-film stress can significantly affect the piezoelectric coefficients and  $k_{\rm t}^2$ .[19,28] Yokoyama et al. showed that the piezoelectric coefficient of the AlN-based FBAR would decrease by increasing the external stress, acting as a tuning knob to modulate the piezoelectric coefficient. The  $k^2$  of the FBAR is also estimated by Yokoyama et al., using the first-principle calculation, which demonstrated a similar trend as the piezoelectric coefficient.[19] We observed a change in the static deformation of the N-polar versus metal-polar FBARs, which

is indicative of the residual stress modulation at the two states. The accumulation of the residual stress will modulate the  $k_{\rm t}^2$  of the AlScN-based FBAR, which results in two operating states depending on the polarization direction of the thin film. The displacements at the resonant frequency and the polarization directions of the FBAR at two polarization states are shown in Figure 4d,e, which demonstrated the change in operating states once the polarization of the AlScN thin film was switched from N-polar to metalpolar state. Detailed investigation of the effect of the release vias and the residual stress profile in the suspended film on the FBAR acoustic properties is a subject of future research.

#### 5. Conclusion

This work reports on ferroelectric highly doped AlN FBAR devices operating at two polarization states. We characterized the hysteresis behavior of the  $Al_{0.7}Sc_{0.3}N$  thin films, showing



www.advancedsciencenews.com



[2] G. Fox, F. Chu, T. Davenport, J. Vac. Sci. Technol. B 2001, 19, 1967,

- [3] C. Zinck, E. Defay, A. Volatier, G. Caruyer, D. P. Tanor, L. Figuiere, in 14th IEEE Int. Symp. on Applications of Ferroelectrics, 2004, IEEE, Piscataway, NJ, USA 2004, https://doi.org/10.1109/ISAF.2004.1418330.
- [4] Z. Yan, J. Liu, Ann. Phys. (Amsterdam, Neth.) 2015, 358, 206.
- [5] A. Khan, K. Chatterjee, B. Wang, S. Drapcho, L. You, C. Serrao, S. Bakaul, R. Ramesh, S. Salahuddin, Nat. Mater. 2015, 14, 182.
- [6] A. Khan, P. Yu, M. Trassin, M. Lee, L. You, S. Salahuddin, Appl. Phys. Lett. 2014, 105, 022903.
- [7] Y. He, B. Bahr, M. Si, P. Ye, D. Weinstein, in 2019 20th Int. Conf. on Solid-State Sensors, Actuators and Microsystems & Eurosensors XXXIII (TRANSDUCERS & EUROSENSORS XXXIII), IEEE, Piscataway, NJ, USA 2019, pp. 717–720, https://doi.org/10.1109/TRANSDUCERS. 2019.8808623.
- [8] S. Lee, V. Lee, S. A. Sis, A. Mortazawi, in 2013 IEEE MTT-S Int. Microwave Symp. Dig. (MTT), IEEE, Piscataway, NJ, USA 2013, https://doi.org/10.1109/MWSYM.2013.6697782.
- [9] J. D. Larson, S. R. Gilbert, B. Xu, in *IEEE Ultrasonics Symp.*, 2004, Vol. 1, IEEE, Piscataway, NJ, USA 2004, pp. 173–177, https://doi. org/10.1109/ULTSYM.2004.1417696.
- [10] Q. Su, B. Zhu, J. Hwan Lee, Z. Bi, K. Shung, Q. Zhou, S. Takeuchi, B. Ho Park, Q. Jia, H. Wang, J. Mater. Res., 2011, 26, 1431.
- [11] M. Z. Koohi, A. Mortazawi, in IEEE Trans. Ultrason. Ferroelectrics Frequency Control, 2020, 67, 1922.
- [12] S. Fichtner, N. Wolff, F. Lofink, L. Kienle, B. Wagner, J. Appl. Phys. 2019, 125, 114103.
- [13] M. A. Caro, S. Zhang, Y. Riekkinen, M. Ylilammi, M. Moram, O. Lopez-Acevedo, J. Molarium, T. Laurila, J. Phys.: Condensed Matter, 2015, 27, 279602.
- [14] A. Ansari, in 2019 IEEE MTT-S Int. Wireless Symp. (IWS), IEEE, Piscataway, NJ, USA 2019, https://doi.org/10.1109/IEEE-IWS.2019. 8804148.
- [15] M. Moreira, J. Bjurström, I. Katardjev, V. Yantchev, Vacuum 2011, 86, 23.
- [16] M. H. S. Alrashdan, A. A. Hamzah, B. Y. Majlis, M. F. Aziz, in 2014 IEEE Int. Conf. on Semiconductor Electronics (ICSE2014), IEEE, Piscataway, NJ, USA 2014, https://doi.org/10.1109/SMELEC.2014. 6920798.
- [17] J. Contreras, H. Kohlstedt, U. Poppe, R. Waser, Appl. Phys. Lett. 2013, 83, 4595.
- [18] B. Tian, Y. Liu, L. Chen, J. Wang, S. Sun, H. Shen, J. Sun, G. Yuan, S. Fusil, V. Garcia, B. Dkhil, X. Meng, J. Chu, Sci Rep, 2016, 5, 18297.
- [19] T. Yokoyama, Y. Iwazaki, T. Nishihara, M. Ueda, in 2012 IEEE Int. Ultrasonics Symp., IEEE, Piscataway, NJ, USA 2012, pp. 551–554, https://doi.org/10.1109/ULTSYM.2012.0137.
- [20] J. Wang, M. Park, A. Ansari, in 2021 34th IEEE Int. Conf. on Micro Electro Mechanical Systems (IEEE MEMS 2021), IEEE, Piscataway, NJ, USA 2021, pp. 214–217, https://doi.org/10.1109/MEMS51782. 2021.9375203.
- [21] J. Wang, M. Park, S. Mertin, T. Pensala, F. Ayazi, A. Ansari, J. Microelectromech. Syst. 2020, 29, 741.
- [22] D. Zhou, J. Xu, Q. Li, F. Cao, X. Dong, J. Muller, T. Schenk, U. Schorder, Appl. Phys. Lett, 2013, 103, 192904.
- [23] M. Pešić, F. P. G. Fengler, L. Larcher, A. Padovani, T. Schenk, E. D. Grimley, X. Sang, J. M. LeBeau, S. Slesazeck, U. Schroeder, T. Mikolajick, Adv. Funct. Mater. 2016, 26, 4501.
- [24] Y. Genenko, J. Glaum, M. Hoffmann, K. Albe, Mater. Sci. Eng.: B 2015, 192. 52.
- [25] D. A. Feld, R. Parker, R. Ruby, P. Bradley, S. Dong, in 2008 IEEE Ultrasonics Symp., IEEE, Piscataway, NJ, USA 2008, pp. 431–436, https://doi.org/10.1109/ULTSYM.2008.0105.

three stages of operation: "wake up," "normal," and "fatigue." Then, the resistance switching behavior of the AlScN MFM capacitors was studied, showing two distinct resistance states caused by polarization inversion. Furthermore, high-performance FBAR devices operating at 3.17 GHz were characterized, showing a very high  $k_t^2$  of 11% and  $Q_{Bode}$  of 572. The FBAR frequency response was modulated upon polarization inversion. The change in the FBAR frequency response is attributed to the residual stress modulation, as well as resistance modulation upon polarization inversion. The change in the residual stress is unique to the anchor design of the FBAR. This work demonstrated different operation states of Al<sub>0.7</sub>Sc<sub>0.3</sub>N-based ferroelectric FBAR, which is controlled by the polarization direction of the thin film. This operating state modulation method paves the way for the realization of high-k<sub>t</sub><sup>2</sup> reconfigurable acoustic filters operating at the superhigh-frequency (SHF) range.

## 6. Experimental Section

The hysteresis behavior of the  $Al_{0.7}Sc_{0.3}N$  thin film was characterized via the measuring of the P-E loop using a modified Sawyer–Tower (ST) circuit.<sup>[29]</sup> The measurement used a triangular wave with a peak voltage of 300 V at 1000 Hz. The  $R_p$ , ESR, and  $C_{fe}$  were directly extracted with the C-V measurement on a Keysight B1505 power device analyzer. The frequency response of the  $Al_{0.7}Sc_{0.3}N$ -based FBARs was measured with a Keysight N54244B PNA network analyzer.

## **Acknowledgements**

The sputtered Al<sub>0.7</sub>Sc<sub>0.3</sub>N and Mo films are provided by the VTT Technical Research Centre of Finland. This work is supported by the NSF CAREER award (ECCS-1944304).The FBAR devices were fabricated at the Institute for Electronics and Nanotechnology (IEN) cleanroom facility at the Georgia Institute of Technology, a member of the National Nanotechnology Coordinated Infrastructure (NNCI).

### **Conflict of Interest**

The authors declare no conflict of interest.

## **Data Availability Statement**

The data that support the findings of this study are available from the corresponding author upon reasonable request.

## Keywords

acoustic resonators, aluminum scandium nitride, film bulk acoustic wave resonators, ferroelectric materials, piezoelectric materials, polarization

Received: January 16, 2021 Revised: March 30, 2021 Published online: April 23, 2021

 M. Pešić, F. Fengler, S. Slesazeck, U. Schroeder, T. Mikolajick, L. Larcher, A. Padovani, in 2016 IEEE Int. Reliability Physics Symp. (IRPS), IEEE, Piscataway, NJ, USA 2016, https://doi.org/10.1109/ IRPS.2016.7574619.



#### www.advancedsciencenews.com



- [26] J. Wang, M. Park, S. Mertin, T. Pensala, F. Ayazi, A. Ansari, in 2020 Joint Conf. of the IEEE Int. Frequency Control Symp. and International Symp. on Applications of Ferroelectrics (IFCS-ISAF), IEEE, Piscataway, NJ, USA 2020, https://doi.org/10.1109/IFCS-ISAF41089.2020. 9234831.
- [27] H. Haag, F. Haemmerle, S. Ben-Yaakov, in Int. Exhibition and Conf. for Power Electronics, Intelligent Motion, Renewable Energy and Energy Management, 2020.
- [28] M. Noorprajuda, M. Ohtsuka, H. Fukuyama, AIP Adv. 2018, 8, 045124.
- [29] C. B. Sawyer, C. H. Tower, Phys. Rev. 1930, 35, 269.